Journal of Catalysis 262 (2009) 206–214

Contents lists available at ScienceDirect

Journal of Catalysis

www.elsevier.com/locate/jcat

Deep hydrodesulfurization over Co/Mo catalysts supported on oxides containing vanadium

Chih-Ming Wang [a], Tseng-Chang Tsai [b], Ikai Wang [a,*]

[a] Department of Chemical Engineering, National Tsing-Hua University, Hsinchu, Taiwan 300, ROC
[b] Department of Applied Chemistry, National University of Kaohsiung, Kaohsiung, Taiwan 811, ROC

ARTICLE INFO

Article history:
Received 2 October 2008
Revised 17 December 2008
Accepted 17 December 2008
Available online 26 January 2009

Keywords:
Hydrodesulfurization
Cobalt–molybdenum sulfides
Dibenzothiophene
4,6-Dimethyldibenzothiophene
Titania
Zirconia
Vanadium oxide
Mixed oxides

ABSTRACT

TiO_2–ZrO_2 and γ-Al_2O_3 supports were modified by impregnation with a vanadium salt. The hydrodesulfurization (HDS) of dibenzothiophene (DBT) and 4,6-dimethyldibenzothiophene (46DMDBT) showed that the selectivity of the hydrogenation (HYD) pathway was greatly increased by this modification. The ratio of HYD to direct desulfurization (DDS) pathway in the HDS of DBT over CoMo/(V_2O_5/TiO_2–ZrO_2) was 3.1 and over CoMo/(V_2O_5/γ-Al_2O_3) it was 0.9. The reactivity of DBT over CoMo/γ-Al_2O_3 was higher than that over CoMo/(V_2O_5/TiO_2–ZrO_2), while the opposite was true for the reactivity of 46DMDBT, which was due to the higher hydrogenation activity, and the more acidic sites of the impregnated V_2O_5 and the mixed metal-oxides supports. Temperature-programmed reduction indicated that CoO–MoO_3 on the TiO_2–ZrO_2 and V_2O_5 modified supports was more reducible and possibly has a different morphology than on γ-Al_2O_3. Furthermore, the results of X-ray photoelectron spectroscopy indicated that the impregnated V_2O_5 affected the interaction between MoS_2 and the supports. Thus, the synergetic effect of binary V–Mo sulfides could induce active sites to facilitate the HYD pathway.

1. Introduction

As environmental consciousness rises, all countries worldwide introduce more stringent legislation to limit the sulfur content of transportation fuels. On the other hand, heavier fractions of petroleum crude are used to make fuels, leading to higher sulfur content in the straight run diesel. Thus, improving the efficiency of the catalysts used in deep hydrodesulfurization (HDS) is one of the most urgent subjects in the petroleum refinery. The commercial HDS catalysts usually contain molybdenum supported on γ-Al_2O_3 promoted with cobalt or nickel. However, the refractory sulfur compounds, typically alkylated dibenzothiophene (DBT), are desulfurized slowly by most commercial HDS catalysts. This is the major challenge for producing ultra low sulfur fuel [1,2].

The activity and selectivity of HDS catalysts are strongly affected by the support. The support not only plays a key role in dispersing the active components and promoters, but also in affecting the morphology and catalytic performance through metal–support interaction. Different metal oxides, including Al_2O_3, TiO_2, and ZrO_2 containing mixed oxides, were studied as HDS catalyst supports [3]. Shimada [4] reported that catalytic performance varies remarkably with the morphology, structure and orientation of MoS_2 clusters on various supports, such as Al_2O_3 and TiO_2. The relative activities of MoS_2 clusters follow the order: "MoS_2 clusters with edge-bonding" > "multi-layered MoS_2 clusters with basal-bonding" > "single-layered MoS_2 clusters with basal-bonding." Segawa et al. [2] synthesized a highly dispersed TiO_2 overlayer on Al_2O_3 by CVD using $TiCl_4$ as precursor. They observed that Mo/TiO_2–Al_2O_3 is more active in the HDS reaction than Mo/γ-Al_2O_3 and Mo/TiO_2. The Mo/TiO_2–Al_2O_3 catalyst had a much higher cyclohexylbenzenes/biphenyls ratio, implying that its HDS mechanism is dominated by the hydrogenation (HYD) pathway instead of the DDS (direct desulfurization without hydrogenation) pathway.

Many articles reported that the reactivity of sulfur compounds depends on their ring size and alkyl substitution positions on the ring [5,6]. Bej et al. [7] reviewed that the HDS catalytic activity of 46DMDBT could be improved by adding different additives into Al_2O_3 or using some supports such as zeolite, TiO_2, and ZrO_2. These additives and supports could enhance the dispersion of the active species (Co, Ni, Mo, and W) and/or increase the number and strength of acidic sites. Ma et al. [8] reported that sterically hindered molecules are preferably desulfurized through the HYD pathway (hydrogenation of aromatic ring and then desulfurization). The effect of steric hindrance of the alkylated DBT can be reduced by means of flat adsorption through π-bonding on the catalyst surface, and by hydrogenation of DBT to hydro-intermediates, in which the methyl group is rotated away from the C–S–C plane.

* Corresponding author. Fax: +886 3 5724725.
E-mail address: ikwang@che.nthu.edu.tw (I. Wang).

0021-9517/$ – see front matter
doi:10.1016/j.jcat.2008.12.012

TiO_2–ZrO_2 mixed metal oxide showed very interesting properties as catalyst support [9]. We have explored the catalytic potential of a ternary oxide, V_2O_5–TiO_2–ZrO_2, as the support for HDS catalysts [10]. Our results showed that at low loading of CoO and MoO_3, V_2O_5–TiO_2–ZrO_2 supported catalysts have a higher hydrogenation activity than the alumina-supported ones. The V_2O_5–TiO_2–ZrO_2 supported catalysts showed lower reduction temperature in temperature-programmed reduction (TPR) and better dispersion of MoO_3 than alumina-supported ones. Moreover, adding V_2O_5 to the TiO_2–ZrO_2 support improved the pore structure of TiO_2–ZrO_2 and avoided the rapid decay of the TiO_2–ZrO_2 catalysts. In this study, we try to improve the hydrogenation activity of the HDS catalysts by impregnating V_2O_5 onto TiO_2–ZrO_2 and γ-Al_2O_3 supports. Those V-promoted catalysts may remove the refractory sulfur compounds more effectively.

2. Experimental

2.1. Catalyst preparation

Home-made TiO_2–ZrO_2 and commercial γ-Al_2O_3 (Strem Chemical, low sodium, 99+% purity), as well as TiO_2–ZrO_2 and γ-Al_2O_3 subsequently modified with vanadia were used as catalyst support. TiO_2–ZrO_2 with a molar ratio of $TiO_2/ZrO_2 = 1/1$ was prepared by co-precipitation [11]. Titanium tetrachloride (SHOWA, 99.9% purity) and zirconium tetrachloride (Lancaster Synthesis, 98% purity) were dissolved in anhydrous alcohol. The solution was mixed with aqueous ammonia (SHOWA, 28%). The gel solution was aged at room temperature for 2 h and then the precipitate was filtered and washed with de-ionized water until no chloride ion was left. The precipitate was dried at 110 °C for 12 h, and then heated to 550 °C at a rate of 2 °C/min and kept at 550 °C in air for 4 h. On the other hand, the γ-Al_2O_3 sample was calcined at 650 °C for 24 h to remove any carbon residue.

The vanadia-overlayered γ-Al_2O_3 and TiO_2–ZrO_2 were prepared by the incipient wetness impregnation method using an aqueous oxalic acid solution of NH_4VO_3 (Merck, >99% purity). After impregnation, the vanadia-overlayered supports were dried at 110 °C for 12 h and then calcined at 550 °C for 4 h. The loading of V_2O_5 was always 5 wt%.

CoO–MoO_3 catalysts were prepared by incipient wetness impregnation. First, $(NH_4)_6Mo_7O_{24}\cdot 4H_2O$ (Merck, >99% purity) was dissolved in a pre-set amount of de-ionized water. After impregnation, the catalyst was dried at 110 °C for 12 h, and then calcined according to the temperature program 50 °C → 400 °C (6 h) → 500 °C (2 h) at a heating rate of 1°C/min. After cooling to room temperature, $Co(NO_3)_2\cdot 6H_2O$ (Merck, >99% purity) was impregnated and calcined according to the same procedure. The loading of CoO and MoO_3 were 2 and 4 wt%, respectively.

2.2. Catalyst characterization

The structures of the synthesized catalysts were examined with a Rigaku RU-H3R X-ray powder diffractometer using Cu$K\alpha$ radiation. TPR and XPS instruments were employed to investigate the species and compositions of the catalysts.

Surface area and pore characteristics were measured with a Micrometrics ASAP 2000 instrument. About 0.3 g of sample was evacuated at 200 °C for 2 h to remove any adsorbed gas and water. Nitrogen adsorption and desorption isotherms were measured at −196 °C. The surface area was determined by the BET method and the pore size distribution was determined by the BJH method.

H_2 and Ar were well mixed and passed through a pre-calcined catalyst loaded in a quartz reactor which was heated with a temperature programmed furnace. The water produced by reduction was adsorbed by a column of zeolite X. The consumption of H_2 along with temperature program was detected by a thermal conductivity detector.

XPS spectra were measured by using a PHI Quantera SXM photoelectron spectrometer with a monochromated A1 anode. The charging effect was minimized by using a charge neutralizer. The C 1s peak at 284.4 eV was taken as the reference. Surface composition was determined from the peak area corrected with a sensitivity factor of Mo 3d, Co 2p, V 2p, S 2p, and S 2s provided by the PHI company instrument. Since the sulfide samples partially re-oxidize upon exposure to air, the colors of the samples changed from black (sulfide) to yellowish brown (oxide). The partially re-oxidized sample, will give a Mo^{5+} signal with a binding energy of 231.0 eV in the Mo $3d_{5/2}$ spectra. In order to avoid the re-oxidization as much as possible, we kept the sulfide samples in a vacuum desiccator during sample transfer to the XPS measurement.

2.3. Catalytic activity test

The HDS of DBT or 46DMDBT was conducted in a continuous flow, fixed bed stainless-steel micro-reactor. A catalyst sample of 2 g was loaded in the reactor, then pre-sulfided under hydrogen pressure (2.96 MPa) with a toluene solution containing 6 wt% CS_2 according to the temperature program 50 °C → 250 °C (16 h) → 350 °C (24 h) at a heating rate of 50 °C/h. The synthetic feed charged into the reactor contains either 1 wt% DBT or 1 wt% 46DMDBT (with sulfur contents of 0.17 or 0.15 wt%, respectively) and 0.4 wt% CS_2 (with sulfur contents of 0.34 wt%) in 98.6% mixed solvent (consisting of 1,2,3,4-tetramethylbenzene, toluene and 1,3,5-trimethylbenzene at a 1:48.6:49 wt ratio). The purpose of adding CS_2 to the feed was to maintain the catalyst in the sulfided states. The catalytic reaction was tested at 300 °C, 3.43 MPa, a feed WHSV of 2–6 h^{-1} and a H_2/HC ratio of 8 mol/mol. During each run, products were periodically sampled and analyzed using a China Chromatograph GC-8700F, equipped with a flame ionization detector and a 0.25 mm × 100 m dimethyl polysiloxane capillary column. A typical GC spectrum of reactor effluent is shown in Fig. 1. Some GC results were further verified by a GC with a sulfur chemiluminescence detector (SCD) and by a GC–MS (GC: HP5890; MASS: HP 5972) equipped with a 0.25 mm × 30 m DB-5 capillary column.

3. Results and discussion

3.1. Catalyst characterization

The loadings of CoO and MoO_3 on all supports, γ-Al_2O_3, V_2O_5 (5 wt%)/γ-Al_2O_3, TiO_2–ZrO_2 and V_2O_5 (5 wt%)/TiO_2–ZrO_2, were 2 and 4 wt%, respectively. No additional peak was present in the X-ray diffraction patterns after loading V_2O_5 and CoO–MoO_3. This implied that V_2O_5 and CoO–MoO_3 were in nano particle size and well-dispersed.

The surface area and pore size of all the studied supports and supported catalysts are listed in Table 1. The surface area, pore volume and average pore size of the γ-Al_2O_3 support (sample γ-Al_2O_3 "S") were 173 m^2/g, 0.43 cc/g and 71 Å, respectively. These numbers changed marginally for the V_2O_5 impregnated (sample V_2O_5/γ-Al_2O_3 "S") and CoO–MoO_3 loaded γ-Al_2O_3 (sample γ-Al_2O_3 "C"). Furthermore, as shown in Fig. 2, the pore size distributions of the γ-Al_2O_3 support before and after impregnation of V_2O_5 or CoO–MoO_3 were almost the same. On the other hand, the surface area, pore volume and average pore size of the mixed metal-oxides TiO_2–ZrO_2 (sample TiO_2–ZrO_2 "S") were 200 m^2/g, 0.24 cc/g and 36 Å, respectively. Compared to the γ-Al_2O_3 support, the surface area of TiO_2–ZrO_2 was larger but its pore volume and average pore diameter were much smaller. Loading CoO–MoO_3 on TiO_2–ZrO_2 (sample TiO_2–ZrO_2 "C") reduced the surface area, but

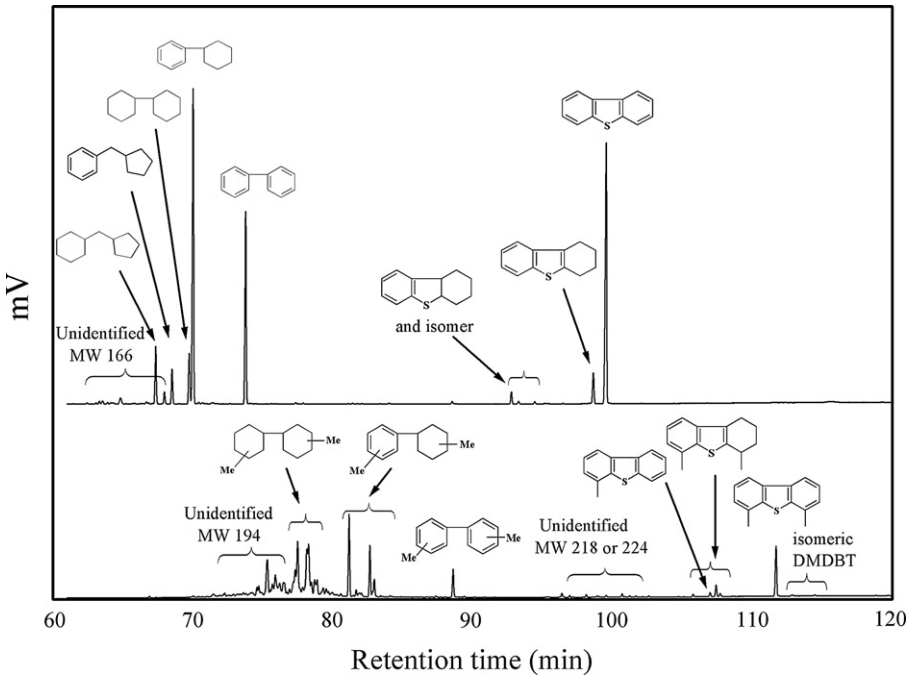

Fig. 1. A typical GC chromatograph of HDS products of reactant DBT and 46DMDBT.

Table 1
Surface area and pore properties of γ-Al_2O_3- and TiO_2–ZrO_2-series supports and supported catalysts.

Supports	γ-Al_2O_3		V_2O_5/γ-Al_2O_3		TiO_2–ZrO_2		V_2O_5/TiO_2–ZrO_2	
Sample type[a]	S	C	S	C	S	C	S	C
CoO/MoO_3 (wt%)	0/0	2/4	0/0	2/4	0/0	2/4	0/0	2/4
Surface area (m^2/g)	173	169	166	157	200	164	106	77
Pore volume (cc/g)	0.43	0.39	0.40	0.36	0.24	0.21	0.20	0.17
Average pore diameter (Å)	71	69	70	69	36	38	54	61

[a] S: support only; C: supported catalyst loaded with 2 wt% CoO–4 wt% MoO_3.

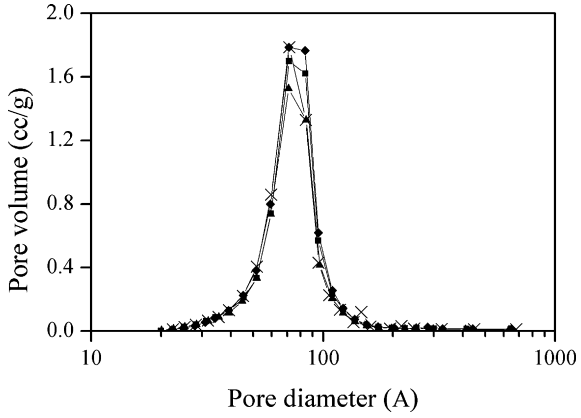

Fig. 2. Pore size distribution of γ-Al_2O_3-series supports: (◆) γ-Al_2O_3; (■) V_2O_5/γ-Al_2O_3; (▲) CoO–MoO_3/(V_2O_5/γ-Al_2O_3); (×) CoO–MoO_3/γ-Al_2O_3.

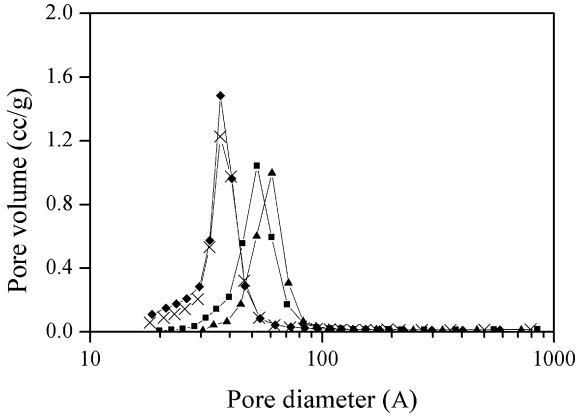

Fig. 3. Pore size distribution of TiO_2–ZrO_2-series supports: (◆) TiO_2–ZrO_2; (■) V_2O_5/TiO_2–ZrO_2; (▲) CoO–MoO_3/(V_2O_5/TiO_2–ZrO_2); (×) CoO–MoO_3/TiO_2–ZrO_2.

the pore characteristics remained the same. However, impregnating V_2O_5 on TiO_2–ZrO_2 (sample V_2O_5/TiO_2–ZrO_2 "S") resulted in a dramatic reduction of the surface area from 200 to 106 m^2/g and an enlargement of the average pore size from 36 to 54 Å. This might be due to a strong interaction between V_2O_5 and TiO_2–ZrO_2 and the unstable structure of TiO_2–ZrO_2 (after another calcination at 550 °C for 4 h, the surface area, pore volume and average pore size of TiO_2–ZrO_2 changed to 170 m^2/g, 0.23 cc/g and 39 Å, respectively). By loading CoO–MoO_3 onto the V_2O_5/TiO_2–ZrO_2 support (sample V_2O_5/TiO_2–ZrO_2 "C"), the surface area and average pore diameter further shifted to 77 m^2/g and 61 Å. The pore size distribution of various TiO_2–ZrO_2 supported catalysts is shown in Fig. 3.

3.2. TPR spectra

TPR spectra of the γ-Al_2O_3 and TiO_2–ZrO_2 supported catalysts are displayed in Fig. 4. The TPR spectrum of CoO–MoO_3/γ-Al_2O_3 showed four main peaks. The reduction of MoO_3 gave two major peaks at 475 °C and 875 °C. According to Thomas et al. [12], the first peak at 475 °C is due to octahedral Mo species and the lat-

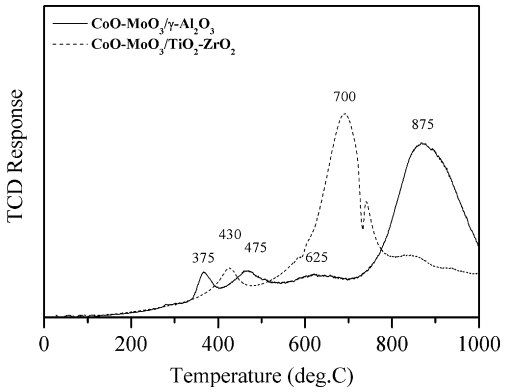

Fig. 4. TPR spectra of different supports: γ-Al_2O_3 (solid); TiO_2–ZrO_2 (dash).

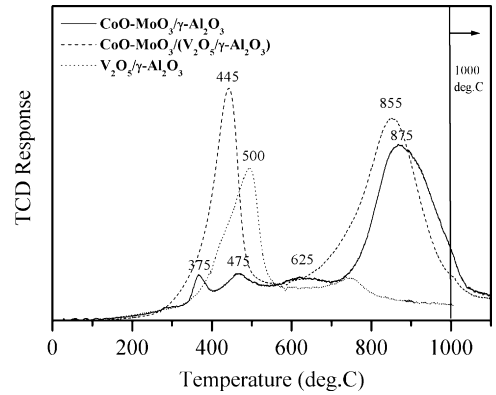

Fig. 5. TPR spectra of γ-Al_2O_3-series supported catalysts: CoO–MoO_3/γ-Al_2O_3 (solid); CoO–MoO_3/(V_2O_5/γ-Al_2O_3) (dash); V_2O_5/γ-Al_2O_3 (dot).

ter one at 875 °C represents tetrahedrally coordinated Mo, bound strongly to the support. The peak at 375 °C probably belongs to the reduction of Co_3O_4 to CoO, while the major reduction peak of CoO to Co overlaps with the reduction peak of MoO_3 at 875 °C [13,14] and the minor peak of 625 °C is the reduction part of surface Co^{2+} ions [13].

The TPR spectrum of CoO–MoO_3/TiO_2–ZrO_2 showed two major peaks at 430 °C and 700 °C and a negative peak at 720 °C. This negative peak might come from the release of a substance by the support or from the formation of a new phase as the TPR temperature was higher than the original calcination temperature of 550 °C [15]. The small TPR peak at 430 °C comes from the reduction of octahedral Mo species and some Co_3O_4. The broad reduction peak at 700 °C is due to tetrahedrally coordinated Mo and some CoO [13,14]. The main peak at 700 °C was 175 °C lower than that of γ-Al_2O_3. This implies that the distinct interaction between the MoO_3 and the TiO_2–ZrO_2 support could form MoO_3 particles with a different morphology (smaller size or single-layered structure) than those on γ-Al_2O_3.

The TPR profiles of vanadium containing supports and catalysts are shown in Figs. 5 and 6. The reduction peaks of V_2O_5 appeared at 500 °C (Fig. 5) and 490 °C (Fig. 6) for the 5 wt% V_2O_5/γ-Al_2O_3 and V_2O_5/TiO_2–ZrO_2 samples, respectively. The TPR profile of CoO–MoO_3/(V_2O_5/γ-Al_2O_3) showed that the reduction peak appears at lower temperature than that of CoO–MoO_3/γ-Al_2O_3 (Fig. 5) and the overall H_2 consumption (peak intensity) was larger than the sum of that of CoO–MoO_3/γ-Al_2O_3 and V_2O_5/γ-Al_2O_3. This indicates that the interlayer V_2O_5 could change the interaction between CoO–MoO_3 and the supports. In the case of the TiO_2–ZrO_2 supported catalyst, there was no notable reduction temperature difference with and without V_2O_5 interlayer, but in spite of that the H_2 consumption of CoO–MoO_3/(V_2O_5/TiO_2–ZrO_2) was greater

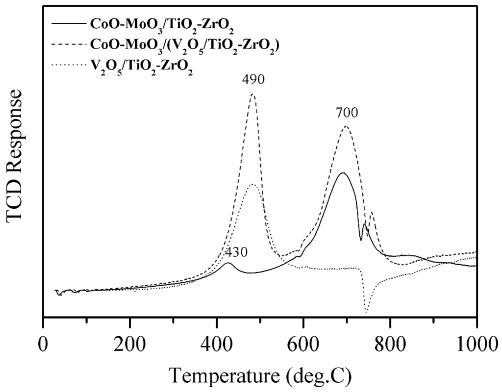

Fig. 6. TPR spectra of TiO_2–ZrO_2-series supported catalysts: CoO–MoO_3/TiO_2–ZrO_2 (solid); CoO–MoO_3/(V_2O_5/TiO_2–ZrO_2) (dash); V_2O_5/TiO_2–ZrO_2 (dot).

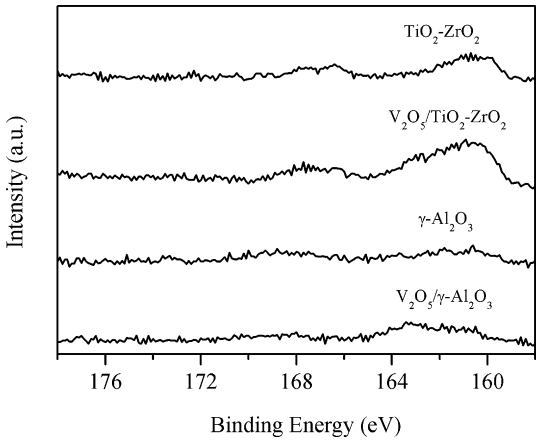

Fig. 7. XPS S 2p spectra of different pre-sulfided supports.

than the sum of that of CoO–MoO_3/TiO_2–ZrO_2 and V_2O_5/TiO_2–ZrO_2 (Fig. 6). The excess hydrogen consumption at lower reduction temperature indicates that the catalysts with impregnated V_2O_5 might cause more octahedral Mo species to form and/or more V_2O_5 to be reduced.

3.3. XPS spectra

3.3.1. Supports

Fig. 7 shows the S 2p XPS spectra of different pre-sulfided supports. The spectrum of pre-sulfided γ-Al_2O_3 showed no S 2p signal and that of pre-sulfided TiO_2–ZrO_2 showed a small sulfur peak. Since TiO_2–ZrO_2 exhibited only a small sulfur peak, there would be no chemical shift on the spectra of Ti 2p or Zr 3d. In addition, the spectrum of pre-sulfided V_2O_5/γ-Al_2O_3 showed a weak sulfur peak, indicating that only a small amount of V_2O_5 was sulfided (combining with curves a and a-s in Fig. 8). Janssens et al. [16] found that the supported vanadium oxide is reducible easier than the bulk one, but they also pointed out that the supported vanadium oxide is only partially sulfided to a V^{3+} oxy-sulfide at 400 °C. Therefore, we can confirm those supported vanadium oxide are only partially sulfided at our pre-sulfided conditions (350 °C). On the other hand, since TiO_2–ZrO_2 was sulfided only slightly, the relatively sharp sulfur peak in the spectrum of pre-sulfided V_2O_5/TiO_2–ZrO_2 indicated that V_2O_5 supported on TiO_2–ZrO_2 may be easier to sulfide than that supported on γ-Al_2O_3.

The oxidic V of V_2O_5 supported on γ-Al_2O_3 and TiO_2–ZrO_2 had V 2p binding energies of 516.5 and 516.0 eV, respectively (Fig. 8). The V 2p peaks of the pre-sulfided supports shifted to lower binding energy, 515.9 and 515.0 eV on γ-Al_2O_3 and TiO_2–ZrO_2, respectively. According to the TPR results, V_2O_5 cannot be reduced

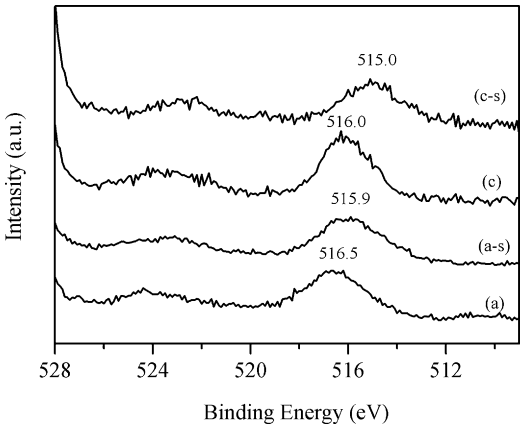

Fig. 8. XPS V 2p spectra of different supports before and after sulfidation: (a) V_2O_5/γ-Al_2O_3; (a-s) pre-sulfided V_2O_5/γ-Al_2O_3; (c) V_2O_5/TiO_2–ZrO_2; (c-s) pre-sulfided V_2O_5/TiO_2–ZrO_2.

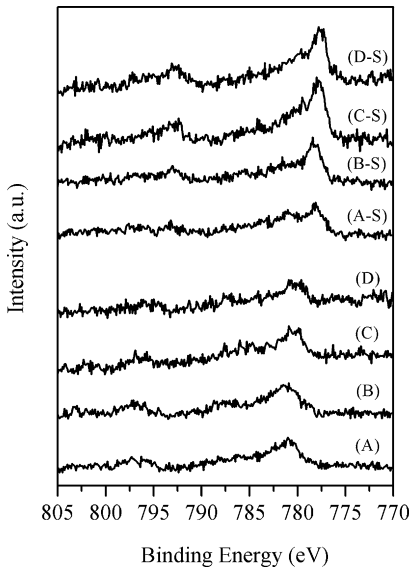

Fig. 9. Co XPS spectra of oxidic and pre-sulfided CoO–MoO_3 catalysts supported on γ-Al_2O_3- and TiO_2–ZrO_2-series supports: (A) V_2O_5/γ-Al_2O_3; (B) γ-Al_2O_3; (C) V_2O_5/TiO_2–ZrO_2; (D) TiO_2–ZrO_2 and their pre-sulfided form (-S). All supports were loaded with 2 wt% CoO–4 wt% MoO_3.

by hydrogen at the pre-sulfiding temperature of 350 °C. Thus, the chemical shift of V 2p was attributed to the sulfidation of V_2O_5.

3.3.2. Catalysts

Figs. 9 and 10 show the Co 2p and Mo 3d (together with S 2s) XPS spectra of the Co–Mo catalysts on different supports, in which (A)–(D) and (A-S)–(D-S) represent oxide states and sulfide states, respectively. The binding energies of Co 2p and Mo 3d of the oxide and sulfide samples, and also the XPS intensity ratios of Co/Mo and S/Mo in the sulfide catalysts are listed in Table 2. Because the intensities of the Co peaks were very weak, the Co/Mo values are not accurate.

The Co peaks in the XPS spectra (A)–(D) of the oxide samples shown in Fig. 9 represent Co $2p_{3/2}$ and Co $2p_{1/2}$ peaks. The Co $2p_{3/2}$ binding energy was 780.0–781.0 eV. The Co $2p_{3/2}$ peaks of the γ-Al_2O_3-series supported catalysts were broader and their binding energies were higher by 1 eV than those of the TiO_2–ZrO_2-series supported ones. This indicates that the structure of CoO–MoO_3 clusters on these two supports might be different. The XPS spectra (A-S)–(D-S) represent the Co sulfide with Co $2p_{3/2}$ binding energies of 777.7–778.1 eV.

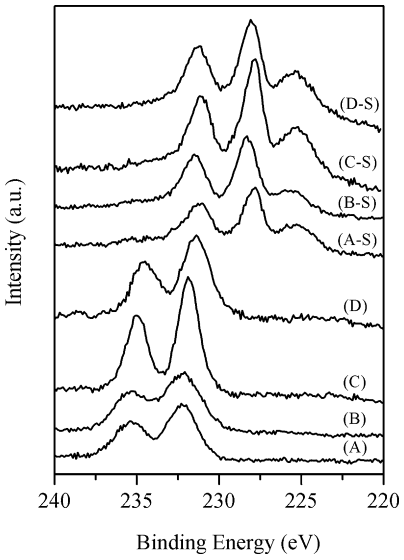

Fig. 10. Mo XPS spectra of oxidic and pre-sulfided CoO–MoO_3 catalysts supported on γ-Al_2O_3- and TiO_2–ZrO_2-series supports: (A) V_2O_5/γ-Al_2O_3; (B) γ-Al_2O_3; (C) V_2O_5/TiO_2–ZrO_2; (D) TiO_2–ZrO_2 and their pre-sulfided form (-S). All supports were loaded with 2 wt% CoO–4 wt% MoO_3.

The Mo peaks of the oxide samples in the spectra (A)–(D) represent Mo $3d_{5/2}$ and Mo $3d_{3/2}$ peaks (Fig. 10). The Mo $3d_{5/2}$ binding energy was 231.4–232.0 eV, which can be assigned to Mo^{+6} of MoO_3 [17]. The Mo $3d_{5/2}$ and Mo $3d_{3/2}$ peaks of the γ-Al_2O_3 supported catalysts were very broad, indicating the presence of multiple Mo(VI) species [18] or a complicated interaction between active components and support [17,19]. On the contrary, the sharp Mo 3d peaks of the TiO_2–ZrO_2-supported catalysts imply uniform structure and chemical characteristics. Moreover, the impregnation of V_2O_5 on the γ-Al_2O_3 support did not affect the MoO_3 structure, but the impregnation on TiO_2–ZrO_2 made the Mo 3d peaks sharper.

As shown in Fig. 10, the XPS spectra varied with different sulfide catalysts. The Mo $3d_{5/2}$ binding energy of all the sulfided catalysts (A-S)–(D-S) changed to 227.7–228.3 eV from the binding energy of 231.4–232.0 eV for the oxidic catalysts (A)–(D). The sulfided species can be assigned to Mo^{4+} of MoS_2 [17]. Furthermore, the XPS peak at 225.2 eV represents the 2s peak of sulfur bonded to Mo, Co, or V. In particular, the Mo 3d peaks shifted by V_2O_5 impregnation to lower binding energies by 0.6 eV and 0.3 eV for V_2O_5/γ-Al_2O_3 and V_2O_5/TiO_2–ZrO_2 supported catalysts, respectively, indicating that the presence of V_2O_5 affected the interaction between MoS_2 and the catalyst support, and/or more reducing type (possible Mo^{3+}) maybe formed.

The V 2p XPS spectra of CoMo/(V_2O_5/γ-Al_2O_3) and CoMo/(V_2O_5/TiO_2–ZrO_2) are shown in Fig. 11. Compared to the XPS spectra of the supports only (Fig. 8), that of supported catalysts (Fig. 11) showed the discrepancy of V 2p binding energy. On V_2O_5/TiO_2–ZrO_2 support with and without CoMo, the V 2p binding energy did not change (515.9–516.0 eV). After sulfidation, vanadium of V_2O_5/TiO_2–ZrO_2 with and without CoMo still represented similar valences. On γ-Al_2O_3 support with and without CoMo, the V 2p binding energy did not change too much (516.3–516.5 eV). After sulfidation, the XPS spectra of supported catalysts (Fig. 11, A-S) showed a lower V 2p binding energy. Therefore, vanadium oxide on γ-Al_2O_3 support became more easily sulfided after loading with CoMo. Furthermore, the V 2p binding energy (515.5 eV mainly) of CoMo/(V_2O_5/γ-Al_2O_3) was higher than that (515.0 eV) of CoMo/(V_2O_5/TiO_2–ZrO_2) among the sulfided samples. The valences of vanadium of CoMo/(V_2O_5/TiO_2–ZrO_2) consisted of V^{4+} and V^{3+}, and those of CoMo/(V_2O_5/γ-

Table 2
Binding energy and atomic ratio of γ-Al_2O_3- and TiO_2–ZrO_2-series supported CoO–MoO_3 catalysts determined with XPS.

CoO–MoO_3 catalysts	Binding energy (eV)				XPS atomic ratio	
	Oxidic		Sulfided		Sulfided	
Support	Mo $3d_{5/2}$	Co $2p_{3/2}$	Mo $3d_{5/2}$	Co $2p_{3/2}$	Co/Mo	S/Mo
γ-Al_2O_3	232.0	781.0	228.3	778.1	0.42	2.64
V_2O_5/γ-Al_2O_3	231.9	781.0	227.7	778.1	0.48	3.50
TiO_2–ZrO_2	231.4	780.0	228.0	777.7	0.65	3.81
V_2O_5/TiO_2–ZrO_2	231.8	780.0	227.7	777.7	0.44	4.04

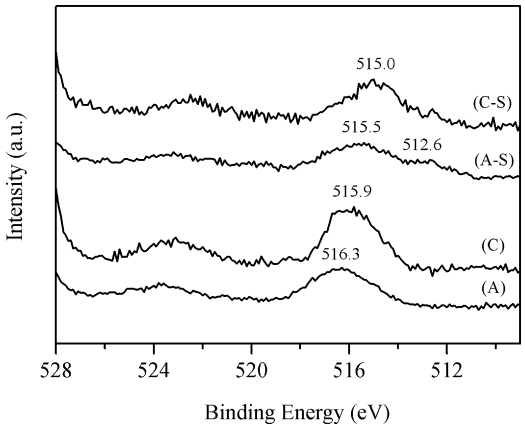

Fig. 11. V XPS 2p spectra of different catalysts before and after pre-sulfidation: (A) CoO–MoO_3/(V_2O_5/γ-Al_2O_3) and pre-sulfided form (A-S); (C) CoO–MoO_3/(V_2O_5/TiO_2–ZrO_2) and pre-sulfided form (C-S).

Al_2O_3) consisted of multiplex valences (a broad peak) and even had some V^{2+} (512.6 eV) forming V–S bond. The different V_xS_y species in different supported catalysts may induce different synergetic effects of V and Mo by the electronic orientated promotion [20].

Furthermore, the peak area of S 2s could be used to estimate the S amount on the catalyst surface. As shown in Table 2, the amounts of the surface S atoms on the TiO_2–ZrO_2-supported catalysts were higher than those on γ-Al_2O_3-supported ones. Upon impregnation of V_2O_5, the amount of surface S atoms in the catalysts was enhanced due to the sulfidation of vanadium oxides. The S/Mo ratio of 2.64 in the γ-Al_2O_3 supported catalyst (Table 2) was smaller than those of the other supported catalysts. Since γ-Al_2O_3 could not be sulfided (Fig. 7), the overall sulfur content came from the CoMo sulfide. From the nominal S/Mo ratio, 2.96 (Mo/Co = 1/0.96, and by the MoS_2 and CoS stoichiometry, a maximum amount theoretically), the γ-Al_2O_3 supported catalyst might possibly possess more S vacancies and undergo HDS reaction predominantly through DDS pathways. The increasing S/Mo ratio of the other supported catalysts was attributed to the increasing degree of sulfidation when adding vanadium and/or going from γ-Al_2O_3 to TiO_2–ZrO_2 (Figs. 7, 8, and 10), and/or forming different morphology of MoS_2 than γ-Al_2O_3. In particular, these vanadium sulfide and titanium sulfide can catalyze the HDS reaction and/or also induce a synergetic effect of binary metal sulfide [20–23]. If the increasing S/Mo ratio was attributed to the distinct morphology of MoS_2 from γ-Al_2O_3, the TiO_2–ZrO_2, V_2O_5/TiO_2–ZrO_2, and V_2O_5/γ-Al_2O_3 supported catalysts could facilitate the formation of fully coordinated sulfur surface, the so-called brim sites [24]. These sites are more favorable for desulfurization through the HYD pathways by hydrogenating thiophene and successively breaking S–C bonds. The change of reaction pathways with the types of support will be discussed in the next section.

Table 3
Products distribution of DBT HDS over CoO–MoO_3 supported on γ-Al_2O_3- and TiO_2–ZrO_2-series.[a]

Supports	γ-Al_2O_3	V_2O_5/γ-Al_2O_3	TiO_2–ZrO_2	V_2O_5/TiO_2–ZrO_2
DBT conversion (%)	99.6	69.7	70.0	70.9
Selectivity (%)				
Desulfurized C_{12} products				
BIP	85.1	53.1	56.1	24.1
PCH	14.4	39.2	34.8	41.6
DIC	0.4	1.1	1.7	8.3
Benzyl-CP	0.1	2.3	3.4	4.2
CP-CH-methane	0.1	1.7	1.5	10.9
Unidentified[b]	0.0	0.7	0.4	3.6
Undesulfurized products				
THDBT (MW 188)	0.0	1.5	1.3	4.8
HHDBT (MW 190)	0.0	0.5	0.5	1.8
Isomeric HHDBT (MW 190)	0.0	0.0	0.2	0.7
HYD/DDS[c]	0.2	0.9	0.8	3.1

[a] Reaction condition: 300 °C, 3.43 MPa, WHSV = 2–6 h^{-1}, H_2/HC = 8 mol/mol.
[b] Unidentified desulfurized C_{12} products, MW 166.
[c] HYD/DDS: selectivity of (1-BIP)/selectivity of BIP.

3.4. Catalyst activity

All the catalyst samples, 2 wt% CoO–4 wt% MoO_3 loaded on different supports, were pre-sulfided by CS_2 as mentioned in Section 2. DBT and 46DMDBT were selected as model reactants and the HDS activity was conducted under the following reaction conditions: 300 °C, 3.43 MPa, WHSV = 2–6 h^{-1}, and H_2/HC = 8 mol/mol. All catalysts showed stable activity up to a time on stream more than 200 h.

3.4.1. HDS of DBT

The HDS results of DBT over various catalysts are shown in Table 3. The products were classified into two groups, "Desulfurized C_{12} products" and "Undesulfurized products." The "Desulfurized C_{12} products" included biphenyl (BIP), phenylcyclohexane (PCH), dicyclohexyl (DIC), isomerization products from PCH or DIC, such as benzylcyclopentane (Benzyl-CP) and (cyclopentyl)cyclohexylmethane (CP-CH-methane), and some unidentified products. The "Undesulfurized products" included four peaks of hydrogenated sulfur-containing compounds, 1,2,3,4-tetrahydro-DBT (THDBT), hexahydro-DBT (HHDBT) and some other products. The GC–MS results (Fig. 1) show that we get one peak for THDBT and three peaks with molecular weight (MW) 190, which are assigned to the *cis*- and *trans*-HHDBT isomers and to its methylated five-membered ring isomer. Moreover, no dodecahydro-DBT product was observed.

The mechanism of HDS can go through two pathways, namely HYD and DDS, as depicted in Fig. 12. As proved experimentally in Table 4, the hydrogenation of BIP to PCH over the V_2O_5/TiO_2–ZrO_2 supported catalyst is very slow and possible even slower in the presence of DBT, as observed for γ-Al_2O_3 supported catalysts [25–27]. Thus, the selectivity of the pathway (HYD/DDS ratio) could be estimated by the yields ratio of (1-BIP)/BIP. As shown in Table 3, the γ-Al_2O_3 supported catalyst possessed a higher activity than the TiO_2–ZrO_2 supported catalyst with a different

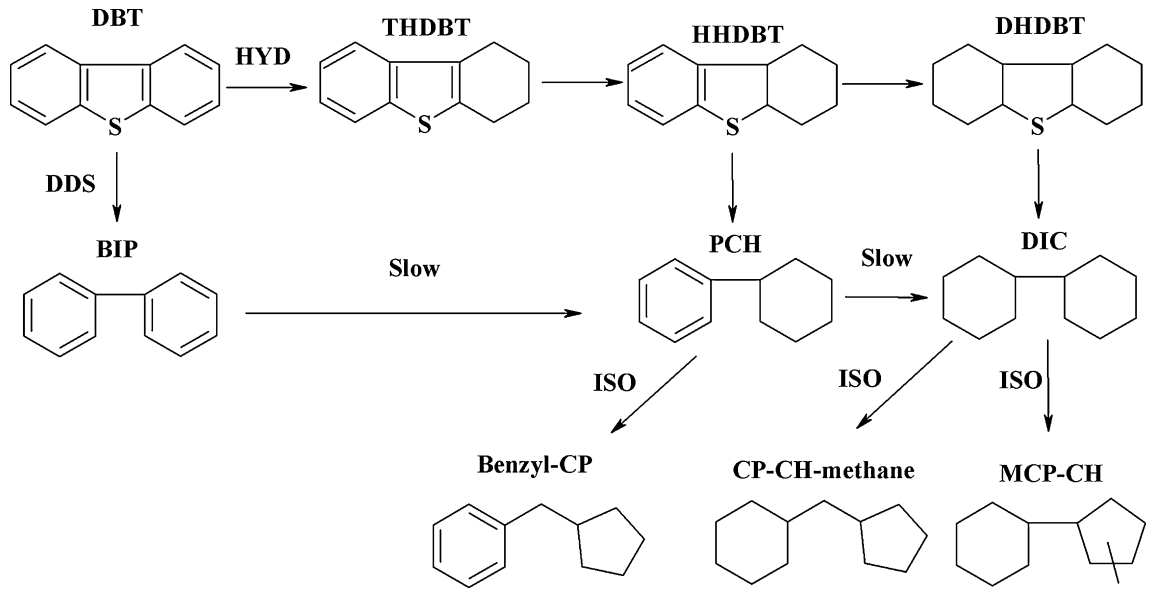

Fig. 12. HDS reaction scheme of DBT on CoO–MoO_3/(V_2O_5/TiO_2–ZrO_2) catalyst.

Table 4
Conversion and products distribution of BIP.[a]

BIP conversion (%)	2.2
Selectivity (%)	
PCH	94.6
DIC	~0.0
CP-CH-methane	5.4

[a] Catalyst: CoO–MoO_3/(V_2O_5/TiO_2–ZrO_2); reaction condition: 300 °C, 3.43 MPa, WHSV = 3 h^{-1}, H_2/HC = 8 mol/mol.

product distribution. The low HYD/DDS ratio (0.2) implies that the sulfur removal over the CoMo/γ-Al_2O_3 catalyst mainly went through the DDS pathway. On the other hand, the HYD/DDS ratio over CoMo/TiO_2–ZrO_2 was 0.8, indicating that both HYD and DDS pathways were equally important. Furthermore, when using the CoMo/TiO_2–ZrO_2 catalyst, a significant amount of partially hydrogenated sulfur compounds appeared in the product, indicating that at least part of sulfur removal went through the HYD pathway. For example, HHDBT as a hydrogenation product of DBT was observed in the HDS product. It can be further hydrogenated to dodecahydro-DBT. DBT can be desulfurized through those hydrogenated intermediates. While HHDBT appeared in the HDS reaction product, dodecahydro-DBT as a very reactive intermediate [27] was not observed. In addition, high yields of isomerization products from PCH or DIC could be attributed to the isomerization activity catalyzed by the acid sites of TiO_2–ZrO_2.

Surprisingly, modification of the γ-Al_2O_3 and TiO_2–ZrO_2 supports by impregnating vanadium greatly changed the selectivity of the reaction products and the reaction pathways. After vanadium modification, the conversion of the V_2O_5/γ-Al_2O_3 supported catalyst reduced to the same level as that of the TiO_2–ZrO_2 supported catalysts. Meanwhile, the HYD/DDS ratio greatly increased from 0.2 to 0.9, which was even higher than that of the TiO_2–ZrO_2 supported catalyst. In particular, the conversion by the DDS pathway strongly decreased (85% to 35%) as revealed in columns 2 and 3 of Table 3. It means that V_2O_5 has a negative effect on the desulfurization ability of the catalyst. Compared with the higher S/Mo of CoMo/(V_2O_5/γ-Al_2O_3) than CoMo/γ-Al_2O_3 in Table 2, we suggested that the lower conversion is due to the decrease of the sulfur vacancies which can desulfurize by the DDS pathway. Since the textural structure of V_2O_5/γ-Al_2O_3 was about the same as that of γ-Al_2O_3, as mentioned in the previous section, the inter-layer

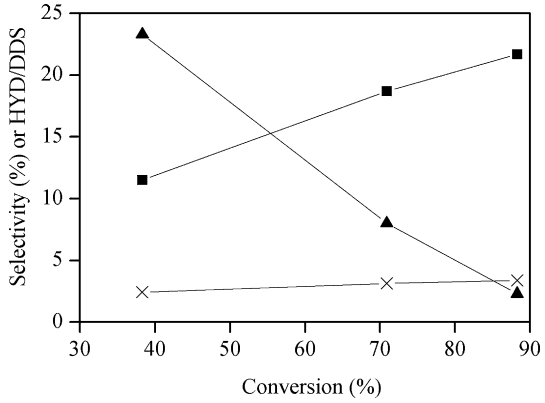

Fig. 13. Plot of selectivity and HYD/DDS ratio versus HDS conversion of DBT over CoO–MoO_3/(V_2O_5/TiO_2–ZrO_2), (×) HYD/DDS; (■) isomerized products from DIC or PCH; (▲) "Undesulfurized products."

of V_2O_5 between CoMo and support should play an important role in affecting the interaction and the morphology of the dispersed CoMo, as will be further discussed later.

The V_2O_5/TiO_2–ZrO_2 supported catalyst had a similar HDS activity as the TiO_2–ZrO_2 supported catalyst, but provided an excellent HYD selectivity, as indicated by a much higher HYD/DDS ratio of 3.1. The selectivities of the isomerized products and the "Undesulfurized products" as well as the HYD/DDS ratios at different conversion levels (by adjusting WHSV at a constant temperature) are given in Fig. 13. With increasing conversion, the selectivity of the isomerized products and the HYD/DDS ratio increased, but the selectivity of the "Undesulfurized products" decreased. The increase of HYD/DDS ratio is due to the slight hydrogenation of BIP at high conversion levels. The high selectivity of isomerized products at high conversion indicates that the HYD products will be further isomerized by the acidic nature of the support. Particularly, the high content of partially hydrogenated intermediates (the "Undesulfurized products") at low conversion levels further verified the HYD reaction pathway over V_2O_5/TiO_2–ZrO_2 supported catalyst.

The HDS of DBT over the V_2O_5/γ-Al_2O_3 and V_2O_5/TiO_2–ZrO_2 supports was also examined. Under the same reaction condition, the HYD/DDS ratios of V_2O_5/γ-Al_2O_3 and V_2O_5/TiO_2–ZrO_2 were 2.4 and 1.7 at conversions of 13.3% and 23.0%, respectively. Fur-

thermore, unlike γ-Al_2O_3 (that has no HDS activity), TiO_2–ZrO_2 showed some HDS activity but deactivated very fast.

Li et al. [28] concluded that the HDS reaction pathway of 46DMDBT and its hydrogenated intermediates occurs by C–S hydrogenolysis rather than by elimination. The desulfurization rate constant increases by one of magnitude when the number of saturated rings in the hydrogenated sulfur compounds increases. Daage and Chianelli [29] proposed a rim-edge model for unsupported catalysts in which sulfur hydrogenolysis takes place on both the rim and edge sites, but DBT hydrogenation occurs exclusively on the rim sites. Topsøe et al. [24] suggested that the so-called brim sites might play a role in the HYD route. In the HDS reaction, hydrogenation first occurs on the brim sites to form hydrogenated intermediates, followed by cleavage of the C–S bond during surface diffusion or during desorption from the brim sites and readsorption on a vacancy of the edge. Nishijima et al. [30] proposed that on an Al_2O_3 support multi-layered MoS_2 clusters are hydrogenolysis-dominated, whereas single layered MoS_2 clusters are hydrogenation-dominated. The structure of the catalyst could affect the catalytic activity and selectivity.

Hubaut [31] reviewed the application of vanadium-based sulfides as hydrotreating catalysts. The synergetic effect of the binary un-supported vanadium-transition metal sulfides is tentatively explained by a mechanism based on a charge transfer leading to change in the energy levels of electronic bands.

Lacroix et al. [21,22] prepared un-supported vanadium sulfide to catalyze different hydrotreating reactions. The pure V_2S_3 from thio-salts had a similar HDS activity as WS_2 and MoS_2, but a superior hydrogenation activity for various cyclic molecules. Moreover, Lacroix et al. [32] further investigated the catalytic properties of unsupported and molybdenum-promoted vanadium sulfide. The catalyst forms a MoS_2-like structure well-dispersed on V_5S_8. The MoV sulfide catalyst performs higher hydrogenating and cracking activity than MoS_2. They explained that in the MoV catalysts, the electron transfer from V species to the surrounding Mo ion may modify the vanadium–sulfur bonding and confer acidity to the mixed MoV site. Furthermore, un-supported Ni–V–S [33] and Fe–V–S [34] also had a better hydrogenation activity than un-supported MoS_2.

The higher reduction temperature of CoO–MoO_3 on γ-Al_2O_3 than TiO_2–ZrO_2, as observed in the TPR study (Fig. 4), implies that the strength of the interaction between CoO–MoO_3 and these two supports is not the same. The interaction could affect the formation of a different particle size or morphology (single- or multi-layered CoO–MoO_3) on these supports. Combining with the HDS results, it might be a possible explanation that single-layered $CoMoS_x$, inducing more HYD pathway selectivity, may be formed on the TiO_2–ZrO_2 support. Moreover, the excess hydrogen consumption presented in Figs. 5 and 6 indicates that CoO–MoO_3 and/or V_2O_5 are easier to reduce. This excess hydrogen consumption could be associated with the higher S/Mo ratio of V-promoted supports in the XPS results. Thus, the CoMo clusters on the V-promoted supports had more chance to form brim sites, and more vanadium sulfide could form. Furthermore, the electronic effects between Mo and the supports with and without V-promotion were not the same by examining the Mo 3d and V 2p chemical shifts on the XPS results.

Accordingly, the higher HYD selectivity over the vanadium-containing catalysts could be due to the single-layered CoMo surface, more vanadium sulfide, and the synergetic electronic effect of the binary vanadium-transition metal sulfides. Since there is no difference of the vanadium valences, as shown in XPS result, on V_2O_5/TiO_2–ZrO_2 with and without CoMo, we suggested the higher hydrogenation activity (HYD/DDS ratio of 3.1) is mainly due to the synergetic electronic effect of the binary vanadium–molybdenum sulfides. If so, the V_2O_5 impregnated supports could be useful in converting those refractory sulfur compounds. This potential is further explored in the following section.

Table 5
Products distribution of 46DMDBT HDS over CoO–MoO_3 supported on γ-Al_2O_3- and TiO_2–ZrO_2-series.[a]

Supports	γ-Al_2O_3	V_2O_5/γ-Al_2O_3	TiO_2–ZrO_2	V_2O_5/TiO_2–ZrO_2
46DMDBT conversion (%)	69.4	76.3	77.9	94.8
Selectivity (%)[b]				
Cracking products	0.0	26.5	7.7	27.8
Desulfurized C_{14} products				
DM-BIPs (MW 182)	10.2	4.4	11.3	2.8
DM-PCHs (MW 188)	77.6	26.7	49.6	16.5
DM-DICs (MW 194)	9.1	27.1	25.1	48.3
Unidentified	0.7	1.0	0.7	0.3
Undesulfurized products				
DBT	0.0	0.3	0.1	0.2
4M-DBT	0.3	1.0	0.5	0.3
TH-DMDBTs (MW 216)	1.5	8.0	2.9	1.9
HH-DMDBTs (MW 218)	0.6	3.3	1.3	1.2
DH-DMDBTs (MW 224)	0.0	1.2	0.3	0.4
Isomeric DMDBTs	0.0	0.6	0.6	0.3

[a] Reaction condition: 300 °C, 3.43 MPa, WHSV = 2–6 h^{-1}, H_2/HC = 8 mol/mol.
[b] The suffix "s" presents the products included themselves and their isomers.

3.4.2. HDS of 46DMDBT

The HDS results of 46DMDBT over various supported catalysts are shown in Table 5. In particular, the conversion of 46DMDBT over CoMo/γ-Al_2O_3 was 69.4%, which was lower than that of DBT of 99.6%. This result was consistent with the conclusion in all investigations [35–37] that the reactivity of DBT is much higher than that of 46DMDBT. However, by carefully examine the product distribution as shown in Table 5, we found that the DDS conversion of 46DMDBT is much lower than that of DBT (85% to 7%) while the HYD conversion is higher (15% to 62%). This indicates that sterically hindered molecules are preferably adsorbed by electron donation (π-bond adsorption) and desulfurized through the HYD pathway [8]. Nevertheless, the conversions of 46DMDBT over CoMo/(V_2O_5/γ-Al_2O_3) and CoMo/TiO_2–ZrO_2 were higher than that of DBT. Especially, over the CoMo/(V_2O_5/TiO_2–ZrO_2) catalyst, the conversion of 46DMDBT was as high as 94.8%, while that of DBT was 70.9%. The DDS conversion of 46DMDBT over the CoMo/(V_2O_5/TiO_2–ZrO_2) catalyst was only near 3% (Table 5). This indicated the higher hydrogenation activity of the CoMo/(V_2O_5/TiO_2–ZrO_2) catalyst could help to desulfurize in a HYD pathway. Besides, it was conjectured that the more acidic sites from the impregnated V_2O_5 and the mixed metal-oxides supports [38] could also transform 46DMDBT to more active intermediates through isomerization, demethylation and C–C bond scission [1,7,39–41].

The HDS products over the CoMo/(V_2O_5/TiO_2–ZrO_2) catalyst consist of 40–50 complicated compounds. As shown in Table 5, the products were classified into three groups, "Cracking products," "Desulfurized C_{14} products" and "Undesulfurized products," in which "Desulfurized C_{14} products," and "Undesulfurized products" can be classified into isomers of different molecular weight. In addition, the material balance over CoMo/(V_2O_5/γ-Al_2O_3, TiO_2–ZrO_2 or V_2O_5/TiO_2–ZrO_2) catalysts was not very accurate because some cracked products were produced, such as toluene, naphthenes, and multi-branched iso-paraffin [41]. The loss amount of the materials was lumped to "Cracking products."

The "Desulfurized C_{14} products" included some non-sulfur compounds of MW 182, 188, and 194, and some unidentified products. The products of MW 182 were dimethyl-BIPs (mainly 33DM-BIP and some 44DM-BIP). The products of MW 188 (consisting of seven GC peaks) were assigned to dimethyl-phenylcyclohexane (DM-PCH) and isomers. The products of MW 194 consisted of three major peaks of 3,3′-dimethyl-1,1′-dicyclohexyl (DM-DIC) and

their isomers. In addition, the "Undesulfurized products" included two 46DMDBT isomers, two demethylation products, 4-methyl-DBT (4M-DBT) and DBT, and some products with MW 216, 218, and 224. From GC–SCD spectra and mass spectra, we suggest that these unidentified products are the pre-hydrogenated and/or isomerization products of DMDBT, such as tetrahydro- (TH-), hexahydro- (HH-) and dodecahydro- (DH-) -DMDBT intermediates. In the HDS of 46DMDBT, the supported catalysts with V_2O_5 impregnated supports had higher activities and produced more cracking products than those without V_2O_5. It indicated that the higher hydrogenation activity and more acidic sites could more efficiently remove those refractory sulfur compounds. This new finding could be useful in the design of new deep desulfurization catalysts for practical refinery application.

4. Conclusion

Vanadium was used to modify TiO_2–ZrO_2 and γ-Al_2O_3 supported CoO–MoO_3 catalysts. It was found that the vanadium-modified CoO–MoO_3 catalyst can greatly enhance the HDS reaction of 46DMDBT.

Two HDS reaction pathways, namely HYD pathway and DDS pathway, were devised for various catalyst systems. The hydrogenation of BIP to PCH over HDS catalysts is always very slow and possible even slower in the presence of DBT. Thus, the selectivity of the pathway (HYD/DDS ratio) could be estimated by the yield ratio (1-BIP)/BIP. Accordingly, the selectivity of the HYD pathway in the HDS of DBT and 46DMDBT was greatly increased by incorporating vanadium into catalyst support. The ratio of HYD to DDS pathway in the HDS of DBT over CoMo/(V_2O_5/TiO_2–ZrO_2) was 3.1 and over CoMo/(V_2O_5/γ-Al_2O_3) it was 0.9. The reactivity of DBT over CoMo/γ-Al_2O_3 was higher than that over CoMo/(V_2O_5/TiO_2–ZrO_2), while the opposite was true for the reactivity of 46DMDBT, which was due to the higher hydrogenation activity, and the more acidic sites of the impregnated V_2O_5 and the mixed metal-oxides supports.

In combining the analytical results of TPR, XPS and the catalyst tests of HDS reaction, we conclude that impregnating of V_2O_5 on γ-Al_2O_3 or TiO_2–ZrO_2 can change the interaction and morphology of $CoMoS_x$ toward a thin-layered cluster on the supports. The HYD activities over the vanadium-containing catalysts, especially CoMo/(V_2O_5/TiO_2–ZrO_2), are attributed to the structural and electronic effects, which could facilitate the HDS reaction of refractory compounds, such as 46DMDBT, effectively. This new design principle should help to design new catalysts for ultra low sulfur diesel production.

Acknowledgments

The authors wish to express their gratitude to G.M. Wei of Chinese Petroleum Corporation for his assistance on the GC–SDC and GC–MS analysis. This work was supported financially by the National Science Council, Taiwan, ROC (NSC 95-2221-E-007-231-MY2).

References

[1] D.D. Whitehurst, T. Isoda, I. Mochida, Adv. Catal. 42 (1998) 345.
[2] K. Segawa, K. Takahashi, S. Satoh, Catal. Today 63 (2000) 123.
[3] G.M. Dhar, B.N. Srinivas, M.S. Rana, M. Kumar, S.K. Maity, Catal. Today 86 (2003) 45.
[4] H. Shimada, Catal. Today 86 (2003) 17.
[5] C.S. Song, Catal. Today 86 (2003) 211.
[6] X.L. Ma, K. Sakanishi, I. Mochida, Ind. Eng. Chem. Res. 33 (1994) 218.
[7] S.K. Bej, S.K. Maity, U.T. Turaga, Energy Fuels 18 (2004) 1227.
[8] X.L. Ma, K. Sakanishi, I. Mochida, Ind. Eng. Chem. Res. 35 (1996) 2487.
[9] B.M. Reddy, A. Khan, Catal. Rev. 47 (2005) 257.
[10] I. Wang, R.C. Chang, J. Catal. 117 (1989) 266.
[11] J. Fung, I. Wang, J. Catal. 130 (1991) 577.
[12] R. Thomas, V.H.J. deBeer, J.A. Moulijn, Bull. Soc. Chim. Belg. 90 (1981) 1349.
[13] P. Arnoldy, J.A. Moulijn, J. Catal. 93 (1985) 38.
[14] P. Arnoldy, M.C. Franken, B. Scheffer, J.A. Moulijn, J. Catal. 96 (1985) 381.
[15] J.C. Wu, C.S. Chung, C.L. Ay, I. Wang, J. Catal. 87 (1984) 98.
[16] J.P. Janssens, A.D. Van Langeveld, J.A. Moulijn, Appl. Catal. A: Gen. 179 (1999) 229.
[17] B.M. Reddy, B. Chowdhury, E.P. Reddy, A. Fernandez, J. Mol. Catal. A: Chem. 162 (2000) 431.
[18] P. Ratnasamy, J. Catal. 40 (1975) 137.
[19] N.K. Nag, J. Phys. Chem. 91 (1987) 2324.
[20] R.R. Chianelli, G. Berhault, P. Raybaud, S. Kasztelan, J. Hafner, H. Toulhoat, Appl. Catal. A: Gen. 227 (2002) 83.
[21] M. Lacroix, N. Boutarfa, C. Guillard, M. Vrinat, M. Breysse, J. Catal. 120 (1989) 473.
[22] C. Guillard, M. Lacroix, M. Vrinat, M. Breysse, B. Mocaer, J. Grimblot, T. des Courieres, D. Faure, Catal. Today 7 (1990) 587.
[23] D. Wang, W. Qian, A. Ishihara, T. Kabe, J. Catal. 203 (2001) 322.
[24] H. Topsøe, B. Hinnemann, J.K. Nørskov, J.V. Lauritsen, F. Besenbacher, P.L. Hansen, G. Hytoft, R.G. Egeberg, K.G. Knudsen, Catal. Today 107–108 (2005) 12.
[25] M. Houalla, N.K. Nag, A.V. Sapre, D.H. Broderick, B.C. Gates, AIChE J. 24 (1978) 1015.
[26] G.H. Singhal, R.L. Espino, J.E. Sobel, G.A. Huff, J. Catal. 67 (1981) 457.
[27] M. Egorova, R. Prins, J. Catal. 225 (2004) 417.
[28] X. Li, A. Wang, M. Egorova, R. Prins, J. Catal. 250 (2007) 283.
[29] M. Daage, R.R. Chianelli, J. Catal. 149 (1994) 414.
[30] A. Nishijima, H. Shimada, T. Sato, Y. Yoshimura, N. Matsubayashi, T. Kameoka, J. Jpn. Petrol. Inst. (Sekiyu Gakkaishi) 32 (1989) 35.
[31] R. Hubaut, Appl. Catal. A: Gen. 322 (2007) 121.
[32] M. Lacroix, C. Guillard, M. Breysse, M. Vrinat, J. Catal. 135 (1992) 304.
[33] P. Betancourt, A. Rives, C.E. Scott, R. Hubaut, Catal. Today 57 (2000) 201.
[34] C.E. Scott, B.P. Embaid, F. Gonzalez-Jimenez, R. Hubaut, J. Grimblot, J. Catal. 166 (1997) 333.
[35] D.R. Kilanowski, H. Teeuwen, V.H.J. deBeer, B.C. Gates, G.C.A. Schuit, H. Kwart, J. Catal. 55 (1978) 129.
[36] M. Houalla, D.H. Broderick, A.V. Sapre, N.K. Nag, V.H.J. deBeer, B.C. Gates, H. Kwart, J. Catal. 61 (1980) 523.
[37] T. Kabe, A. Ishihara, Q. Zhang, Appl. Catal. A: Gen. 97 (1993) L1.
[38] R.C. Chang, I. Wang, J. Catal. 107 (1987) 195.
[39] M.V. Landau, D. Berger, M. Herskowitz, J. Catal. 159 (1996) 236.
[40] T. Isoda, S. Nagao, X. Ma, Y. Korai, I. Mochida, Energy Fuels 10 (1996) 1078.
[41] P. Michaud, J.L. Lemberton, G. Pérot, Appl. Catal. A: Gen. 169 (1998) 343.